Phase Amplitude Coupling workflow for mapping EEG signals to standard brain networks

Mariano Fernandez-Corazza
Instituto LEICI
UNLP - CONICET
La Plata, Argentina
marianof.corazza@ing.unlp.edu.ar

Evan Hathaway
BEL Company
University of Oregon
Eugene, Oregon, USA
ephathaway@gmail.com

Kyle Morgan
BEL Company
Eugene, Oregon, USA
kyle.morgan@bel.company

Roma Shusterman
BEL Company
Eugene, Oregon, USA
roma.shusterman@bel.company

Dante Andrinolo Instituto LEICI
UNLP - CONICET
La Plata, Argentina
dante.andrinolo@alu.ing.unlp.edu.ar

Phan Luu
BEL Company
University of Oregon
Eugene, Oregon, USA
phann.luu@bel.company

Carlos Muravchik
Instituto LEICI
UNLP - CONICET
La Plata, Argentina
carlosm@ing.unlp.edu.ar

Don Tucker
BEL Company
University of Oregon
Eugene, Oregon, USA
don.tucker@bel.company

Abstract— **Human brain mapping or neuroimaging plays a pivotal role in understanding the intricacies of the human brain and paving the way for potential therapeutic interventions. Studying the standard brain networks, typically obtained from fMRI, provide valuable insights into the fundamental organization of the human brain. In this work we present a workflow for processing electroencephalography (EEG) signals to determine the correlations of the phase-amplitude coupling (PAC) of the standard brain networks during a given time-window. We validate this pipeline with synthetic signals on realistic head models of two subjects with the ultimate goal of studying the changes of these networks during different sleep stages. The proposed workflow consists of: mapping the signals to the source space, averaging per Brodmann Area (BA), low and high pass filtering, computing the modulation index per low-high frequency pair, generating surrogate data to obtain significance thresholds, obtaining the significant PAC signals, computing the signal and noise covariance matrices, removing the model bias, and applying confirmatory factor analysis (CFA) to determine the relevance of each standard brain network. We included the novelty of using CFA instead of principal component analysis as done in previous studies. We tested the workflow with synthetic signals, and it performed as expected. Next steps will be fine-tuning it and improving its robustness before processing real signals during sleep that we already have collected for the two subjects of the head models used here.**

Keywords—brain networks, phase amplitude coupling, confirmatory factor analysis, electroencephalography inverse problem.

I. Introduction

Human brain mapping or neuroimaging plays a pivotal role in understanding the intricacies of the human brain and unlocking its mysteries. The motivation behind this field stems from the fundamental desire to comprehend the complex processes underlying cognition, perception, emotion, and behavior, thereby advancing our knowledge of human nature and paving the way for potential therapeutic interventions. With the synergic use of modalities such as functional magnetic resonance imaging (fMRI) or diffusion tensor imaging (DTI), researchers can identify brain regions involved in memory, attention, language, and decision-making. For example, a study used fMRI to investigate the neural mechanisms underlying episodic memory retrieval, shedding light on the interplay between different brain regions during this process [1]. In another study, diffusion tensor imaging (DTI) was employed to reveal disrupted white matter connectivity in patients with schizophrenia, offering insights into the underlying neural pathology [2].

Studying the standard brain networks, such as the default mode network (DMN), the attention networks or the somatomotor network (SMN) (also known as central executive network), holds immense relevance and motivation in the field of neuroscience. These networks, typically obtained from fMRI, provide valuable insights into the fundamental organization of the human brain and are crucial for understanding various cognitive processes and their dysregulation in neurological and psychiatric disorders. Recent findings have shed light on the impact of the standard brain networks, on sleep and its associated processes. These networks play crucial roles in regulating sleep architecture, sleep-related cognitive processes, and sleep disorders. Research has shown that the activity and connectivity within the DMN are altered during different stages of sleep, including rapid eye movement (REM) sleep and non-rapid eye movement (NREM) sleep. For instance, a study demonstrated increased DMN connectivity during REM sleep, suggesting a potential role in dream generation and self-referential mental processes during this sleep stage [3]. The ventral attention network (VAN), also known as salience network, is responsible for detecting salient stimuli and initiating attentional processes, and it also shows interactions with sleep. Studies have found that the VAN undergoes changes in functional connectivity and activity across sleep stages. For instance, a study revealed decreased VAN connectivity during NREM sleep, suggesting a reduction in the detection of salient stimuli and a shift toward more internally focused processes during sleep [4]. Furthermore, the frontoparietal network (FPN), associated with higher-order cognitive functions and cognitive control, has implications for sleep and sleep disorders. Disruptions in FPN connectivity have been observed in sleep disorders such as insomnia. A study found that individuals with chronic insomnia exhibited altered FPN connectivity patterns during wakefulness, highlighting the potential involvement of this network in sleep disturbances and cognitive impairments associated with insomnia [5]. Moreover, recent studies have explored the interplay between these networks and sleep disorders such as sleep apnea, such as altered connectivity between the DMN and VAN in individuals with obstructive sleep apnea, suggesting impaired cognitive and attentional processes during wakefulness and sleep in these individuals [6].

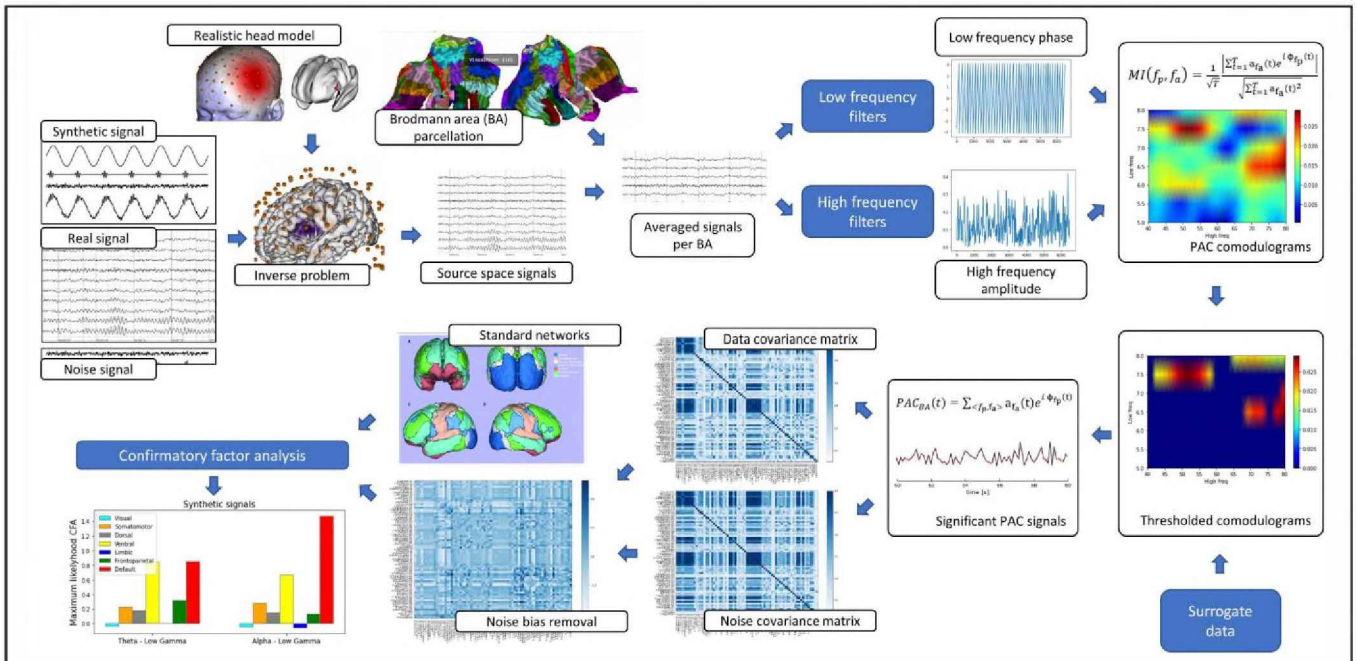

Figure 1: Proposed workflow. The signals of the electrodes (either synthetic, real or noise only) are mapped to the source space by solving the EEG inverse problem. The signals are averaged per Brodmann Area (BA) and then filtered for different low and high frequency bands, extracting the low frequency phase and the high frequency amplitude. For each combination of a low frequency and a high frequency the PAC strength is computed generating one comodulogram per BA. Based on the generation of surrogate data, thresholds of significance are determined for each low-high frequency pair. The surviving pairs are used to generate the significant PAC signals, one per BA. The covariance matrix is obtained for the data and for the noise only signals. The biases of the model are removed by projecting the data covariance matrix to the space orthogonal to the first noise eigenvector. The data convariance matrix without the noise bias is combined with the brain standard network parcellation in the confirmatory factor analysis, that returns the relevance of each network in the processed signals.

Collectively, these recent findings highlight the significant impact of the standard brain networks, including the DMN, VAN, and SMN, on sleep architecture, sleep-related cognitive processes, and sleep disorders. Understanding the dynamic interactions between these networks during sleep can provide insights into the underlying mechanisms of sleep-related functions and disorders, potentially guiding the development of targeted interventions for sleep-related cognitive impairments and sleep disorders. However, analyzing brain networks during sleep using fMRI has the practical difficulty that fMRI is extremely noisy and uncomfortable, as well as being highly expensive. Thus, there is a need for techniques that can analyze these networks with less invasive measurement technologies such as magnetoencephalography (MEG) or electroencephalography (EEG).

MEG consists in measuring the subtle magnetic fields generated by brain activity of large groups of synchronized, localized and aligned neurons. This technique can capture the brain dynamics more efficiently than fMRI but it is still expensive and mostly capture activity that is not perpendicularly aligned to the scalp cortex. EEG has also very high temporal resolution and is much less expensive than fMRI or MEG. It also measures the electromagnetic phenomena produced by neuronal activation, but sensing the electric potential on the scalp with a set or array of electrodes. It has the disadvantage that the electric potential is highly sensitive to the geometry and electrical conductivity of the head tissues. In the context of sleep study, it has the advantage of being relatively comfortable to wear allowing sleep data acquisition in a context (a comfortable bed, silent environment, horizontal position and with good movement freedom) much more like natural sleep than fMRI or MEG.

Phase-amplitude coupling (PAC) is a neurophysiological phenomenon that involves the coupling of different frequencies of neural oscillations in the brain. Specifically, it refers to the modulation of the amplitude of high-frequency oscillations by the phase of low-frequency oscillations. PAC has been widely studied as it reflects the dynamic interactions between distinct brain regions and plays a crucial role in various cognitive processes. One of the most relevant findings using PAC is its involvement in memory and learning. For instance, hippocampal-cortical PAC increased during memory retrieval, suggesting that phase-amplitude coupling might support memory consolidation and information transfer between different brain regions [7]. Moreover, PAC has been implicated in attention and perception. It has been observed that PAC between theta and gamma oscillations is modulated during attentional tasks, reflecting the coordinated communication between brain areas involved in selective attention [8]. This phenomenon highlights the role of PAC in coordinating neural activity and enhancing information processing during cognitive tasks. Furthermore, PAC abnormalities have been linked to various neurological and psychiatric disorders. For example, disruptions in PAC have been reported in conditions such as epilepsy [9] and schizophrenia [10]. These findings suggest that PAC may serve as a potential biomarker for neurological and psychiatric conditions, aiding in diagnosis and treatment.

In this work we present our own implementation of a workflow for processing electroencephalography (EEG) signals to determine the correlations of the phase-amplitude

coupling (PAC) of the standard brain networks during a given time-window. We validate this pipeline with synthetic signals. The purpose of this study is to present the workflow, that will be used in a next stage to process more than 20 subjects during sleep to discover how the standard networks activate or deactivate during the different sleep stages.

II. WORKFLOW

In this section we describe the proposed workflow, which is mostly based on a previous study [11], but adapted to EEG and modified where we found some issues. At the final step we use confirmatory factor analysis (CFA) instead of principal component analysis (PCA) to obtain the predominant brain networks that explain the PAC data. Fig. 1 shows a block diagram of the entire workflow, which was implemented in Python and is described in detail below.

A. Head Modeling

Based on structural magnetic resonance (MR) and computed tomography images of two healthy adults (S1: male, Caucasian, 28 years old and S2: female, Asian, 23 years old) we built two realistic head models using BEL's EMAD toolbox [12]. The head is segmented into seven tissues (scalp, skull, cerebrospinal fluid, eyeballs, gray matter, white matter, and internal air) and we assigned to them literature conductivity values (0.35, 0.01, 1.79, 1.55, 0.33, 0.25 and 0 S/m, respectively). EMAD was also used to parcellate the cortical surface into 9600 oriented dipoles and to corregister an EGI Geodesic Sensor net with 256 electrodes. The electromagnetic problem was solved using BEL's hexahedral finite element method (FEM) solver HexaFEM, generating a lead field matrix L with the resulting electric potential at each electrode produced by each dipolar source.

B. Synthetic signal generation

We generated two synthetic PAC signals with two different low and high frequencies, one with theta – low gamma PAC and another with alpha – low gamma PAC. The PAC signals were generated using the formula described in [13]:

$$X_{f_p}(t) = K_{f_p}\sin(2\pi f_p t), \quad (1)$$

$$X_{f_a}(t) = A_{f_a}(t)sin(2\pi f_a t), \quad (2)$$

with

$$A_{f_a}(t) = K_{f_a}\frac{(1-\chi)\,sin(2\pi f_p t-\phi_c)+\chi+1}{2}, \quad (3)$$

where $X_{f_p}(t)$ is the phase signal, $X_{f_a}(t)$ is the amplitude signal, f_p is the phase low frequency, f_a is the amplitude high frequency, K_{f_p} is the amplitude of $X_{f_p}(t)$, K_{f_a} determines the amplitude of $X_{f_a}(t)$, $(1-\chi)$ with $\chi \in [0,1]$ is the coupling strength, and ϕ_c is the coupling phase. Then, the PAC signal at the source space is:

$$X(t) = X_{f_a}(t) + X_{f_p}(t) + \epsilon(t), \quad (4)$$

where $\epsilon(t)$ is the PAC noise term.

The chosen parameters for the VAN were $f_p = 6Hz$ (theta band), $f_a = 62Hz$, $K_{f_p} = 10uV$, $K_{f_a} = 2uV$, $\chi = 0.2$; and for the DMN were $f_p = 10Hz$ (alpha band), $f_a = 47Hz$, $K_{f_p} = 9uV$, $K_{f_a} = 3uV$, $\chi = 0.2$. Note that $\epsilon(t)$ is a source of noise that affects the original PAC signal, which we defined as Gaussian noise with $\sigma = 0.001$.

For each head model, the two PAC signals were applied to 4 arbitrarily selected dipoles, two at distant regions of the VAN and two at distant regions of the DMN. We selected dipoles with very similar Montreal Neurological Institute (MNI) coordinates for the two subjects. The final MNI coordinates (x,y,z) were:

- Subject S1, VAN (theta) source 1: -35, 6, 14
- Subject S1, VAN (theta) source 2: 64, -27, 30
- Subject S1, DMN (alpha) source 1: -50, -62, 29
- Subject S1, DMN (alpha) source 2: 4, 59, -2
- Subject S2, VAN (theta) source 1: -35, 4, 9
- Subject S2, VAN (theta) source 2: 63, -29, 25
- Subject S2, DMN (alpha) source 1: -52, -64, 29
- Subject S2, DMN (alpha) source 2: 4, 62, -3

The synthetic EEG signals $Y(t)$ at the sensors were generated by multiplying the source PAC signals in (4) by the leadfield of each selected dipole, as shown in (5):

$$Y(t) = l(r_1^{van})^T \otimes X^{van}(t) + l(r_2^{van})^T \otimes X^{van}(t) + l(r_1^{dmn})^T \otimes X^{dmn}(t) + l(r_2^{dmn})^T \otimes X^{dmn}(t) + N(t), \quad (5)$$

where $l(r)$ is the leadfield vector with the potential at all electrodes produced by a dipolar source located at r, r_1^n and r_2^n are the locations of selected sources 1 and 2 of network n, $\otimes$ means the outer product, and $N(t)$ is a second source of noise at the sensors, with an SNR of 50dB in this work.

C. Source space mapping

The EEG data is mapped to the brain space to obtain a signal per dipolar source. This inverse solution was estimated using the classical standardized low-resolution brain electromagnetic tomography algorithm (sLORETA) [14] implemented in BEL's Sourcerer Suite. sLORETA is one of the most popular inverse solvers due to its algorithmic simplicity and unbiased nature [15]. The formulation is:

$$s(r,t) = \frac{l(r)^T\left(LL^T+\alpha I\right)^{-1}}{\sqrt{l(r)^T\left(LL^T+\alpha I\right)^{-1}l(r)}}\,Y(t) \quad (6)$$

where α is a hyperparameter, I is the identity matrix and $s(r,t)$ is the source waveform estimate of dipole r at time t. Formulation in (6) is repeated for each possible source of activity. The hyperparameter was selected by visual inspection of a few samples of the source reconstructions and then it remained fixed for the rest of them ($\alpha = 0.01$).

Source localizations were run for each subject and for each dipole. To reduce the source space and make the whole workflow computationally tractable, the mean waveform per Brodmann Area (BA) was obtained by averaging the individual waveforms of all dipoles of each BA. This averaging was done considering the orientation of each dipole because if dipoles are oriented in opposite directions, the source waveforms are reflected and thus, a simple averaging can lead to the suppression of the signals. At this point we have 76 signals, one per BA.

D. Low and High frequency filtering.

Each BA signal is filtered to obtain low and high frequency signals. The bandpass pass filters for the low frequencies are 4th order Butterworth covering the theta band (5-8 Hz) and the alpha band (8-12 Hz) with a 0.5 Hz step and 0.5 Hz of bandwidth, giving a total of 15 low frequency bins. The band pass filters for the high frequencies are also 4th order Butterworth covering the low Gamma (40-80Hz) with a logarithmic step (following [11]) and 30Hz of bandwidth. In our work, the final number of bins were 25 for the low Gamma band. The phases $\phi_{f_p}(t)$ and the amplitudes $a_{f_a}(t)$ are extracted from the low pass signals and the high pass signals respectively, after building the complex envelope via Hilbert Transform [16].

E. PAC signals and comodulograms

For each BA a comodulogram is generated by computing the modulation index (MI) for each low and high frequency pair of bins:

$$MI(f_p, f_a) = \frac{1}{\sqrt{T}} \frac{\left|\sum_{t=1}^{T} a_{f_a}(t) e^{i\,\phi_{f_p}(t)}\right|}{\sqrt{\sum_{t=1}^{T} {a_{f_a}}^2(t)}}, \quad (7)$$

where T is the number of time samples. The MI formula can be read as the normalized module of the complex vector that is generated by the sum of the complex PAC signal vectors over the whole time window. Thus, if the low-frequency phases and high-frequency amplitudes are coupled, the vectors are mostly aligned and the resulting MI is be large.

A comodulogram shows the strength of the PAC for all pairs of low frequency and high frequency bin combinations, as seen in Fig. 1 top-right corner. A hypothesis test is required to establish the significance of the MI. The MI statistical distribution is needed though hard to derive. Thus, it is suggested the use of surrogate data [17].

F. Surrogate data and thresholding

200 sets of surrogate data are generated by using the same amplitudes of the data, but with random phases. The surrogate comodulograms are used to create significance thresholds for each low-high frequency bin pairs. In Florin et al, 2015 they generate only one significance threshold for all frequency pairs instead of one threshold per frequency pair [11]. This results in the lower frequencies having more chances to survive, due to the 1/f behavior of the brain spectrum, as explained in Gohel et al 2016 [17]. The threshold for each frequency pair was set as p = 0.05 before Bonferroni correction.

The data comodulograms (one per BA) are thresholded based on the surrogate data (see Fig. 1, right-bottom) and then, the PAC signal for each BA with only the significant information is rebuilt following:

$$PAC_{BA}(t) = \sum_{<f_p, f_a>} a_{f_a}(t) e^{i\,\phi_{f_p}(t)}, \quad (8)$$

where $< f_p, f_a >$ are the surviving low-high frequency pairs.

The surrogate data generation is the most time-consuming task because almost the whole workflow has to be repeated 200 times, although it can be parallelized. In an Intel(R) Xeon(R) CPU E5-2603 v4 @ 1.70GHz with 6 cores and 132 GB of RAM the whole workflow with parallelization takes around 2 hours.

G. Covariance matrix

At this point there is one PAC signal per BA. The sample covariance matrix is computed to understand the networks of the brain. However, this covariance matrix might include spurious correlations given by the source localization process, which is not 100% focused resulting in leakage (i.e., the activity obtained on one dipole is not independent of the signal of the neighbor dipole). To reduce this bias, a white Gaussian noise (WGN) only signal at the sensors is generated and processed following steps C to G. The result is a noise only covariance matrix (see Fig. 1, bottom center). Then, the principal mode of the noise matrix singular value decomposition is removed from the signal covariance matrix using orthogonal projection. Note that the noise matrix can also change for a different realization. We made the noise data length large enough (10 seconds), until we saw that it was stable for different realizations. This is another improvement we made over Florin et al 2015 workflow.

H. Brain parcellation into networks

The EMAD segmentation software provides the MNI coordinates of each dipole. This information was used to map each dipole to one of the seven functional brain networks of the Yeo et al, 2011 atlas [18]: visual, somatomotor, dorsal attention, ventral attention, limbic, frontoparietal and default mode networks. These networks constitute an atlas that is very popular and standard in fMRI data analysis.

I. Confirmatory factor analysis

We used the confirmatory factor analysis to see how much these networks explain the PAC covariance matrix. CFA decomposition is similar to PCA decomposition with the difference that in CFA the modes are predefined (in this case the Yeo et al 2011 networks) instead of being obtained as the eigenvectors of the PCA decomposition. We followed a standard CFA procedure that minimizes the maximum likelihood equation [19]:

$$F_{ML} = \ln|\Lambda\,\Omega\,\Lambda^{\mathrm{T}} + I - diag(\Lambda\,\Omega\,\Lambda^{T})| + tr(R(\Lambda\,\Omega\,\Lambda^{T} + I - diag(\Lambda\,\Omega\,\Lambda^{T}))^{-1}) - ln(R) - p \quad (8)$$

where Λ is the matrix containing the predefined modes, i.e., the mapping between the BA parcellation and the standard brain network parcellation, Ω is the unknown 7x7 diagonal matrix with the weights of each network, I is the identity matrix, R is the data covariance matrix with noise bias removed, described in section II.G, and p is the number of unknown variables (7 in this case).

III. Examples

In this section we show the results of processing synthetic data using two different realistic head models. Fig. 2 shows the results of the CFA, for both theta-gamma and alpha-gamma PACs for subjects S1 and S2. It can be observed that the VAN and DFM are the predominant modes, and that the DFM is larger for the alpha band. Note that both modes are also seen in the other band (VAN in alpha and DFM in theta). In the discussion section we give a possible reason for this.

IV. Discussion

A. Differences with respect to Florin et al 2015.

In the process of replicating Florin et al 2015 pipeline, we found some issues that we think they can be improved. Here we highlight the most important modifications we introduced in our pipeline. First, the thresholds of significance were

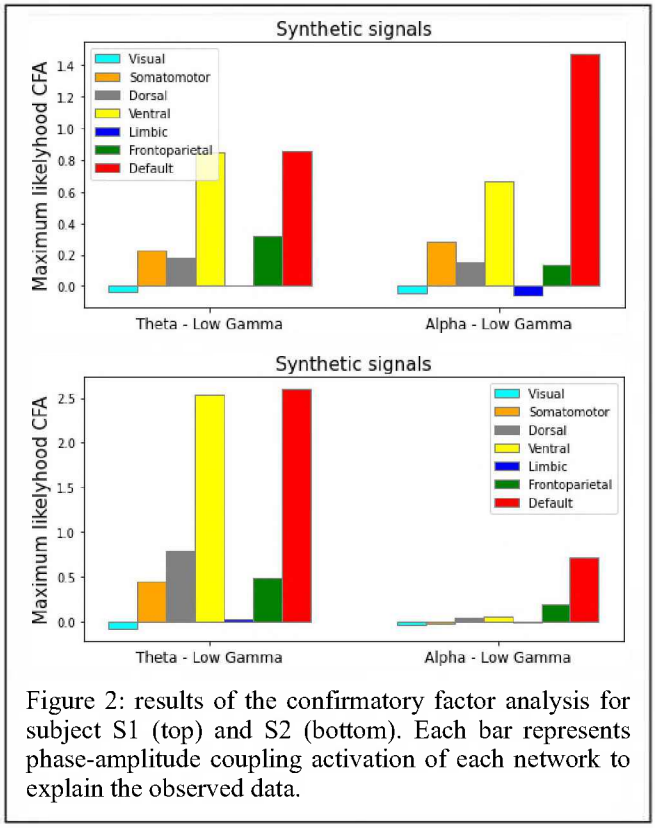

Figure 2: results of the confirmatory factor analysis for subject S1 (top) and S2 (bottom). Each bar represents phase-amplitude coupling activation of each network to explain the observed data.

applied to the whole comodulograms (all frequencies), instead of computing one threshold per low-high frequency pair, as done in another study [17]. This results in a bias towards low frequencies having more significance, which is seen in Fig. 2 from Florin et al., 2015. We replicated this effect by processing only noise, where this bias was clearly seen. Second, the surrogate data was computed using the phase of a noise only signal but the amplitude of the data, instead of using both the phase and amplitudes of noise only signals. The approach we used preserves the power spectrum of the original data [20]. One final relevant difference is that we used confirmatory factor analysis instead of blind principal component analysis. CFA is more suitable when the projection vectors can be defined a-priori, as it occurs in this case with the standard brain networks.

B. *Results*

Although the results are preliminary, there are some interesting findings to describe. First, the networks are not 100% decoupled, even for synthetic data. One reason can be the inherent spatial smoothing produced when solving the inverse problem. However, this effect should be mostly mitigated by the orthogonal to the noise space projection. We also plan to use more spatially selective inverse solvers such as beamforming [15] or multiple sparse priors [21]. Another cause of this coupling is produced by the fact that the BA parcellation of the brain is not aligned with the network parcellation, meaning that some averaged signals per BA belong to different networks.

Another finding is that the results change significantly when a higher noise is used (results not shown). We found that the effects of the noise added to the PAC signals is more relevant than the noise added to the sensors. Finally, another finding is that there is some cross-frequency crosstalk. This means that a network with a simulated PAC for one low frequency band (for instance theta) also appears as a strong network in the other low frequency bands. Note for instance in Fig. 2 that the DMN is as strong as the VAN for the Theta-Gamma coupling, where the VAN should be stronger. The expected reason of this effect is described in the following section.

C. *Limitations*

One effect we found is that when considering only the phase of a low frequency bin, if there is PAC with a high frequency amplitude, there will necessarily be PAC with the lower harmonics of the low frequency. For instance, if there is strong PAC between the phase of 10Hz and the amplitude of 60Hz, there will also be strong PAC between the phase of 5Hz and the amplitude of 60Hz. This effect was not mentioned in the literature, and we will further study it. Another effect we found is that the solutions are very sensitive to the noise. In this work we had to lower the simulated noise levels significantly to get robust solutions. This high sensitivity to noise will be carefully analyzed before processing real data. Finally, the CFA lacks of a "null-hypothesis network". This implies that even pure random noise will result in some network activation. This issue is also present when doing PCA as it is done in the previous PAC works, because even for noise only signals (and even if projected to the orthogonal to noise space), there will be some residual that will produce one principal component. We think that this issue must be carefully addressed in future works.

Overall, the workflow for processing PAC with brain signals, either fMRI, MEG or EEG is complex and subject to many sources of errors and it is still a developing technique, without lack of controversies. For instance, Gohel et al 2016 criticized Florin et al 2015 by not using a correct significancy thresholding [17]. Thus, Gohel et al 2016 tested different ways of generating the surrogate data. Florin et al 2017 replied back Gohel et al 2016 with a short note, defending themselves from Gohel et al 2016 critiques [22]. Moreover, there is a very recent work with the current pitfalls of the different stages of the PAC analysis [20]. Each step of the workflow has different variants and parameters that must be fine-tuned because most of them are conceptually sound. We believe that more simulations using different synthetic data types must still be carried out to gain confidence in the workflow. However, we consider this work as a relevant first milestone of a novel end-to-end workflow that combines what we found as the best solutions proposed in previous works.

V. Conclusions

We proposed an end-to-end PAC analysis workflow to process EG data considering what we believe are the best approaches described in previous works. We included the novelty of using CFA instead of PCA, which we believe it is a major advantage of the proposed workflow. We tested it with synthetic signals and the full workflow performed as expected. Next steps will be fine-tuning it and improving its robustness before processing real signals during sleep that we already have collected for the two subjects of the head models used here.

Acknowledgment

This work was supported by the ANPCyT PICT 2019-0701, UNLP I-257, CONICET PIP 11220200101515CO grants.

References

[1] M. D. Rugg and K. L. Vilberg, "Brain networks underlying episodic memory retrieval," *Curr. Opin. Neurobiol.*, vol. 23, no. 2, pp. 255–260, Apr. 2013, doi: 10.1016/j.conb.2012.11.005.

[2] M. P. van den Heuvel, E. T. Bullmore, and O. Sporns, "Comparative Connectomics," *Trends Cogn. Sci.*, vol. 20, no. 5, pp. 345–361, May 2016, doi: 10.1016/j.tics.2016.03.001.

[3] F. Siclari *et al.*, "The neural correlates of dreaming," *Nat. Neurosci.*, vol. 20, no. 6, pp. 872–878, Jun. 2017, doi: 10.1038/nn.4545.

[4] V. I. Spoormaker *et al.*, "The neural correlates and temporal sequence of the relationship between shock exposure, disturbed sleep and impaired consolidation of fear extinction," *J. Psychiatr. Res.*, vol. 44, no. 16, pp. 1121–1128, Dec. 2010, doi: 10.1016/j.jpsychires.2010.04.017.

[5] X.-J. Dai *et al.*, "Plasticity and Susceptibility of Brain Morphometry Alterations to Insufficient Sleep," *Front. Psychiatry*, vol. 9, Jun. 2018, doi: 10.3389/fpsyt.2018.00266.

[6] H. Khazaie *et al.*, "Functional reorganization in obstructive sleep apnoea and insomnia: A systematic review of the resting-state fMRI," *Neurosci. Biobehav. Rev.*, vol. 77, pp. 219–231, Jun. 2017, doi: 10.1016/j.neubiorev.2017.03.013.

[7] N. Axmacher *et al.*, "Intracranial EEG Correlates of Expectancy and Memory Formation in the Human Hippocampus and Nucleus Accumbens," *Neuron*, vol. 65, no. 4, pp. 541–549, Feb. 2010, doi: 10.1016/j.neuron.2010.02.006.

[8] R. T. Canolty and R. T. Knight, "The functional role of cross-frequency coupling," *Trends Cogn. Sci.*, vol. 14, no. 11, pp. 506–515, Nov. 2010, doi: 10.1016/j.tics.2010.09.001.

[9] C. A. Schevon *et al.*, "Evidence of an inhibitory restraint of seizure activity in humans," *Nat. Commun.*, vol. 3, p. 1060, Sep. 2012, doi: 10.1038/ncomms2056.

[10] A. Korzeniewska, M. Mańczak, M. Kamiński, K. J. Blinowska, and S. Kasicki, "Determination of information flow direction among brain structures by a modified directed transfer function (dDTF) method," *J. Neurosci. Methods*, vol. 125, no. 1–2, pp. 195–207, May 2003, doi: 10.1016/S0165-0270(03)00052-9.

[11] E. Florin and S. Baillet, "The brain's resting-state activity is shaped by synchronized cross-frequency coupling of neural oscillations," *Neuroimage*, vol. 111, pp. 26–35, May 2015, doi: 10.1016/j.neuroimage.2015.01.054.

[12] K. Li, X. Papademetris, and D. M. Tucker, "BrainK for Structural Image Processing: Creating Electrical Models of the Human Head," *Comput. Intell. Neurosci.*, vol. 2016, pp. 1–25, 2016, doi: 10.1155/2016/1349851.

[13] T. T. K. Munia and S. Aviyente, "Time-Frequency Based Phase-Amplitude Coupling Measure For Neuronal Oscillations," *Sci. Rep.*, vol. 9, no. 1, p. 12441, Aug. 2019, doi: 10.1038/s41598-019-48870-2.

[14] R. D. Pascual-Marqui, "Standardized low-resolution brain electromagnetic tomography (sLORETA): technical details.," *Methods Find. Exp. Clin. Pharmacol.*, vol. 24 Suppl D, no. SUPPL. D, pp. 5–12, 2002, [Online]. Available: http://www.ncbi.nlm.nih.gov/pubmed/12575463.

[15] K. Sekihara and S. S. Nagarajan, *Adaptive Spatial Filters for Electromagnetic Brain Imaging*. Berlin: Springer, 2008.

[16] J. Aru *et al.*, "Untangling cross-frequency coupling in neuroscience," *Curr. Opin. Neurobiol.*, vol. 31, pp. 51–61, Apr. 2015, doi: 10.1016/j.conb.2014.08.002.

[17] B. Gohel *et al.*, "Evaluation of Phase-Amplitude Coupling in Resting State Magnetoencephalographic Signals: Effect of Surrogates and Evaluation Approach," *Front. Comput. Neurosci.*, vol. 10, Nov. 2016, doi: 10.3389/fncom.2016.00120.

[18] B. T. Thomas Yeo *et al.*, "The organization of the human cerebral cortex estimated by intrinsic functional connectivity," *J. Neurophysiol.*, vol. 106, no. 3, pp. 1125–1165, Sep. 2011, doi: 10.1152/jn.00338.2011.

[19] F. Yang-Wallentin, K. Joreskog, and H. Luo, "Confirmatory Factor Analysis of Ordinal Variables With Misspecified Models," *Struct. Equ. Model. A Multidiscip. J.*, vol. 17, no. 3, pp. 392–423, Jul. 2010, doi: 10.1080/10705511.2010.489003.

[20] G. J. Jurkiewicz, M. J. Hunt, and J. Żygierewicz, "Addressing Pitfalls in Phase-Amplitude Coupling Analysis with an Extended Modulation Index Toolbox," *Neuroinformatics*, vol. 19, no. 2, pp. 319–345, Apr. 2021, doi: 10.1007/s12021-020-09487-3.

[21] K. Friston *et al.*, "Multiple sparse priors for the M/EEG inverse problem," *Neuroimage*, vol. 39, no. 3, pp. 1104–1120, 2008, doi: 10.1016/j.neuroimage.2007.09.048.

[22] E. Florin and S. Baillet, "Commentary: Evaluation of Phase-Amplitude Coupling in Resting State Magnetoencephalographic Signals: Effect of Surrogates and Evaluation Approach," *Front. Comput. Neurosci.*, vol. 12, Apr. 2018, doi: 10.3389/fncom.2018.00026.